



1 **Mid-Pliocene Atlantic Meridional Overturning Circulation simulated in PlioMIP2**

2 Zhongshi Zhang¹, Xiangyu Li¹, Chuncheng Guo², Odd Helge Otterå^{2,3}, Kerim H. Nisancioglu⁴, Ning Tan⁵,
3 Camille Contoux⁶, Gilles Ramstein⁶, Ran Feng⁷, Bette L. Otto-Bliesner⁸, Esther Brady⁸, Deepak Chandan⁹,
4 W. Richard Peltier⁹, Michiel L. J. Baatsen¹⁰, Anna S. von der Heydt¹⁰, Julia E. Weiffenbach¹⁰, Christian
5 Stepanek¹¹, Gerrit Lohmann^{11,12}, Qiong Zhang¹³, Qiang Li¹³, Mark A. Chandler¹⁴, Linda E. Sohl¹⁴, Alan M.
6 Haywood¹⁵, Stephen J. Hunter¹⁵, Julia C. Tindall¹⁵, Charles Williams¹⁶, Daniel J. Lunt¹⁶, Wing-Le Chan¹⁷,
7 Ayako Abe-Ouchi¹⁷

8

- 9 1. Department of Atmospheric Science, School of Environmental studies, China University of Geoscience, Wuhan, 430074, China
10 2. NORCE Norwegian Research Centre, Bjerknes Centre for Climate Research, 5007 Bergen, Norway
11 3. Center for Early Sapiens Behaviour, 5007 Bergen, Norway
12 4. Department of Earth Science and Bjerknes Centre for Climate Research, University of Bergen, 5007 Bergen, Norway
13 5. Key Laboratory of Cenozoic Geology and Environment, Institute of Geology and Geophysics, Chinese Academy of Sciences,
14 Beijing 100029, China
15 6. Laboratoire des Sciences du Climat et de l'Environnement, LSCE/IPSL, CEA-CNRS-UVSQ, Université Paris-Saclay, F-91191
16 Gif-sur-Yvette, France
17 7. Department of Geosciences, University of Connecticut, Storrs, USA
18 8. Climate and Global Dynamics Laboratory, National Center for Atmospheric Research, Boulder, USA
19 9. Department of Physics, University of Toronto, Toronto, Canada
20 10. Institute for Marine and Atmospheric research Utrecht (IMAU), Department of Physics, Utrecht University, Utrecht, The
21 Netherlands.
22 11. Alfred Wegener Institute – Helmholtz Centre for Polar and Marine Research, Bremerhaven, Germany
23 12. Institute for Environmental Physics, University of Bremen, Bremen, Germany
24 13. Department of Physical Geography and Bolin Centre for Climate Research, Stockholm University, Stockholm, Sweden
25 14. CCSR/GISS, Columbia University, New York, USA
26 15. School of Earth and Environment, University of Leeds, Woodhouse Lane, Leeds, West Yorkshire, LS29JT, UK
27 16. School of Geographical Sciences, University of Bristol, Bristol, UK.
28 17. Atmosphere and Ocean Research Institute (AORI), University of Tokyo, Kashiwa, Japan

29

30 Correspondence: Zhongshi Zhang(zhongshi.zhang@cug.edu.cn)

31

32

33

34

35

36

37

38

39

40



41 **Abstract**

42 In the Pliocene Model Intercomparison Project phase 2 (PlioMIP2), coupled climate models have been used
43 to simulate an interglacial climate during the mid-Piacenzian warm period (mPWP, 3.264 to 3.025 Ma).
44 Here, we compare the Atlantic Meridional Overturning Circulation (AMOC), poleward ocean heat transport
45 and sea surface warming in the Atlantic simulated with these models. In PlioMIP2, all models simulate an
46 intensified mid-Pliocene AMOC. However, there is no consistent response in the simulated Atlantic ocean
47 heat transport, or the depth of the Atlantic overturning cell. The models show a large spread in the simulated
48 AMOC maximum, the Atlantic ocean heat transport, as well as the surface warming in the North Atlantic.
49 Although a few models simulate a surface warming of ~8–12 °C in the North Atlantic, similar to the
50 reconstruction from Pliocene Research, Interpretation and Synoptic Mapping (PRISM), most models
51 underestimate this warming. The large model-spread and model-data discrepancies in the PlioMIP2
52 ensemble does not support the hypothesis that an intensification of the AMOC, together with an increase in
53 northward ocean heat transport, is the dominant forcing for the mid-Pliocene warm climate.

54

55

56 **1. Introduction**

57 The mid-Piacenzian warm period (mPWP, 3.264–3.025 Ma) was a recent period of sustained warmth in
58 geological history, with land-sea distribution, topography and levels of greenhouse gases being comparable
59 to today (Dowsett et al., 2010, 2016; Haywood et al., 2010, 2016a). The estimated global mean temperature
60 during the mPWP was 2–4°C higher than the pre-industrial (e.g., Dowsett et al., 2010, 2016; Haywood et al.,
61 2010, 2016a), and the atmospheric CO₂ level was above 400ppmv (Badger et al., 2013). Thus, the mPWP
62 climate is often thought of as a plausible test case that has the potential to provide insights for our future
63 climate (e.g., Zubakov and Borzenkova, 1988; Haywood et al., 2016b; Burke et al., 2018).

64 To understand the mPWP climate, the Pliocene Modelling Intercomparison Project (PlioMIP) phase 1
65 was launched in 2010 (Haywood et al., 2010). The major forcing considered in PlioMIP1 was an increase
66 (compared to pre-industrial) in the atmospheric CO₂ level to 405 ppmv, combined with a modern land-sea
67 distribution (Haywood et al., 2013). Based on the PlioMIP1 simulations (e.g., Chan et al., 2011; Bragg et al.,
68 2012; Contoux et al., 2012; Kamae and Ueda, 2012; Stepanek and Lohmann, 2012; Zhang et al., 2012;
69 Chandler et al., 2013; Rosenbloom et al., 2013), numerous studies were carried out to investigate various
70 aspects of the warm mid-Pliocene climate, including: the Hadley and Walker circulations (Sun et al., 2013;
71 Corvec and Fletcher, 2017); tropical cyclones (Yan et al., 2016); monsoon circulations (Zhang et al., 2013a,



72 2016; Li et al., 2018); mid-latitude westerly winds (Li et al., 2015); Arctic sea ice (Howell et al., 2016);
73 energy balance of the climate system (Hill et al., 2014); and climate sensitivity (Hargreaves and Annan
74 2016). These PlioMIP1 simulations showed that the global annual mean surface air temperature (SAT) was
75 1.9–3.6°C warmer than pre-industrial in the multi-model ensemble mean (Haywood et al., 2013), while the
76 strength of Atlantic Meridional Overturning Circulation (AMOC) was similar to the pre-industrial (Zhang et
77 al., 2013b). However, when compared to marine and terrestrial reconstructions, there was a large model-data
78 discrepancy in the North Atlantic (Dowsett et al., 2012, 2013; Haywood et al., 2013) and the land realm of
79 the Northern Hemisphere (Salzmann et al. 2013). The simulated increases in the sea surface temperatures
80 (SSTs) in the North Atlantic were ~4–6°C less than the reconstructions (Dowsett et al., 2012, 2013;
81 Haywood et al., 2013; Salzmann et al. 2013). Since the PlioMIP1 simulations (Zhang et al., 2013b, 2013c)
82 did not support a stronger Pliocene AMOC (compared to preindustrial) and an inferred enhancement of
83 Atlantic northward ocean heat transport (OHT) suggested by proxies (Dowsett, 1992; Raymo et al., 1996), it
84 was difficult to explain the reconstructed strong surface warming in the high-latitude North Atlantic during
85 the mid-Pliocene.

86 To further understand the mPWP climate and to improve upon the model-data discrepancy, the PlioMIP
87 phase 2 was initiated in 2016 (Haywood et al., 2016a). PlioMIP2 employs state-of-the-art boundary
88 conditions from the Pliocene Research, Interpretation and Synoptic Mapping (PRISM) version 4 (Dowsett et
89 al., 2016a), and focuses on the KM5c interglacial period in the mid-Pliocene (Haywood et al., 2016a). The
90 PRISM4 boundary conditions include reconstructed ocean bathymetry and land-ice surface topography, and
91 also incorporate Pliocene soils and lakes (Dowsett et al., 2016; Haywood et al., 2016a). The most important
92 change in boundary conditions in the northern high latitudes is the closure of the Canadian Archipelago and
93 the Bering Strait (Haywood et al., 2016a). When incorporating the PRISM4 boundary conditions in
94 PlioMIP2, the global annual mean SAT increases by 1.7–5.2°C relative to the pre-industrial, with a
95 multi-model mean SAT increase of 3.2°C (Haywood et al., 2020). In the Arctic, simulated annual mean SAT
96 increases by 3.7–11.6 °C compared to the pre-industrial, with a multi-model mean increase of 7.2 °C (de
97 Nooijer et al., 2020).

98 In this study, we compare the simulated AMOC in PlioMIP2, in order to further address the question
99 whether an intensified AMOC and enhanced Atlantic OHT can explain the reconstructed North
100 Atlantic-Arctic sea surface warming during the mPWP. In section 2, we briefly introduce the models
101 participated in PlioMIP2. In section 3, we compare the simulated AMOC and Atlantic OHT between
102 PlioMIP1 and PlioMIP2. In section 4, we investigate the relationship between the simulated AMOC



103 response and changes in North Atlantic SST. Finally, the results are discussed and summarized in section 5.

104

105 **2. Introduction of models used in PlioMIP2**

106 In this study, we analyze simulations with the fifteen models that have participated and provided the
107 simulated AMOC results to PlioMIP2 (Table 1). They are CCSM4 (Feng et al., 2020), CCSM4-UoT
108 (Chandan and Peltier, 2017; 2018), CCSM4-Utrecht (Baatsen et al. 2020, in prep), CESM1.2 (Feng et al.,
109 2020), CESM2 (Feng et al., 2020), COSMOS (Stepanek et al., 2020), EC-Earth3-LR (Döscher et al., 2020,
110 in prep), GISS-E2-1-G, HadCM3 (Hunter et al., 2019), IPSLCM5A2 (Tan et al., 2020), IPSLCM5A (Tan et
111 al., 2020), IPSLCM6A-LR (Lurton et al., 2020), MIROC4m (Chan and Abe-Ouchi, 2020), NorESM1-F (Li
112 et al., 2020), and NorESM-L (Li et al., 2020). All fifteen models have performed simulations according to
113 the PlioMIP2 experimental protocol (Haywood et al., 2016). They provide the pre-industrial control
114 experiment (*pi-E280*) and the mid-Pliocene experiment (*midPliocene-Eoi400*) as a minimum. In the
115 mid-Pliocene experiment, a land-sea mask with the Arctic gateways closed and an atmospheric CO₂ level of
116 400ppmv are used. The atmospheric CO₂ level is in line with the very latest high-resolution proxy
117 reconstruction based on Boron isotopes for ~3.2 Ma (Chalk et al. 2018). More details on the individual
118 models and experimental design are introduced in a recent synthesis study (Haywood et al., 2020) and
119 several individual modeling studies (Chandan and Peltier, 2017; 2018; Hunter et al., 2019; Chan and
120 Abe-Ouchi, 2020; Döscher et al., 2020; Feng et al., 2020; Li et al., 2020; Lurton et al., 2020; Stepanek et al.,
121 2020; Tan et al., 2020). In addition to these fifteen models, MRI-CGCM (Kamae et al., 2016) and
122 HadGEM3 have taken part in PlioMIP2. However, MRI-CGCM has not provided the AMOC results to the
123 PlioMIP2 database, while HadGEM3 has not used the land-sea distribution condition with the Arctic
124 gateways closed.

125 Of the fifteen PlioMIP2 models used here, six of them also took part in PlioMIP1. They are CCSM4,
126 COSMOS, HadCM3, IPSLCM5A, MIROC4m and NorESM-L. However, all these six models have
127 submitted new pre-industrial control experiments to the PlioMIP2 database, and some of these pre-industrial
128 experiments have been extended. CCSM4 has also been used by other modelling groups, as CCSM4-UoT
129 and CCSM-Utrecht. Therefore, the pre-industrial AMOC maximums and depths in PlioMIP2 are slightly
130 different to the values in PlioMIP1.

131

132 **3. Simulated AMOC and OHT**

133 **3.1 Simulated AMOC in PlioMIP2**



134 The PlioMIP2 models produce reasonable simulations for the pre-industrial AMOC. The pre-industrial
135 AMOC maximums (the maximum of the Atlantic meridional overturning streamfunction) range from ~10 to
136 28 Sv ($1 \text{ Sv} \equiv 10^6 \text{ m}^3 \text{ s}^{-1}$; Table 1, Fig. 1). The multi-model median value of the AMOC maximums is 19.8
137 Sv, which is comparable to the observational estimates of $18.7 \pm 2.1 \text{ Sv}$ (Kanzow et al. 2010). The depths of
138 the Atlantic overturning cell range from 2300 m to 3800 m.

139 In PlioMIP2, the models show that the maximum AMOC is enhanced by 1% to 53% in the
140 mid-Pliocene, relative to the pre-industrial (Table 1, Fig. 1). The median value of the enhancement is 19%.
141 Seven models (CCSM-UoT, COSMOS, GISS-E2-1-G, HadCM3, IPSLCM5A, IPSLCM5A2,
142 IPSLCM6A-LR) show insignificant changes in the depth of the mid-Pliocene Atlantic overturning cell (with
143 depth changes of less than 100 m), when compared to the pre-industrial. However, five models, CCSM4,
144 CESM1.2, CESM2, EC-Earth3-LR and MIROC4m, simulate a shoaling of the Atlantic overturning cell for
145 the mid-Pliocene, with a shoaling of ~1190m, ~1330m, ~820m, ~350 m and ~440 m. On the other hand,
146 three models, CCSM4-Utrecht, NorESM1-F, and NorESM-L, simulate a deeper mid-Pliocene Atlantic
147 overturning cell with increases in the depth of ~540m, ~1590 m and ~1330 m (Fig. 1, 2).

148 Compared to PlioMIP1 (Zhang et al., 2013b), the simulated AMOC responses to Pliocene boundary
149 conditions are different in PlioMIP2 (Fig. 2). In PlioMIP1, there was no consistent increase in the maximum
150 strength of the AMOC, while there was a consistent shoaling of the Atlantic overturning cell. However, in
151 PlioMIP2, there is a consistent increase in the maximum strength of the AMOC, while there is no consistent
152 change in the depth of Atlantic overturning cell.

153

154 3.2 Simulated Atlantic OHT in PlioMIP2

155 As expected from the intensified AMOC, most models simulate an enhanced Atlantic OHT (averaged
156 between 30°S and 80°N) in the mid-Pliocene experiments relative to the pre-industrial (Table 1, Fig. 3). The
157 increases range from 4% to 39%. The largest enhancement is found in the simulation with IPSLCM5A2,
158 while the smallest one is simulated with NorESM1-F. In contrast, six models, CCSM4, CESM1.2, CESM2,
159 GISS-E2-1-G, MIROC4m and NorESM-L show a decrease (ranged from -1% to -17%) in Atlantic OHT.

160 Obviously, there is no linear relationship between the intensification in AMOC and the changes in mean
161 Atlantic OHT in the PlioMIP2 simulations (Fig. 2b). For example, GISS-E2-1-G and IPSLCM6A-LR both
162 simulate increases of 24% in the AMOC maximum. However, GISS-E2-1-G shows a decrease in mean
163 Atlantic OHT by -1%, while IPSLCM6A-LR shows an increase of 29%. CCSM4 and CCSM4-Utrecht also
164 show the same increase of 11% in the AMOC maximum, but opposite responses in the mean Atlantic OHT.



165 This large model-spread in PlioMIP2 suggests that the responses within AMOC strength and Atlantic
166 northward OHT are highly model-dependent.

167

168 **4. Simulated North Atlantic sea surface warming**

169 In PlioMIP2, the simulated mid-Pliocene global annual mean SST is between 1.2 and 4.0 °C warmer
170 than the pre-industrial. Most models show that the strongest sea surface warming appears in the mid-to-high
171 latitude North Atlantic (Fig. 4, 5). The median of multi-model ensemble shows that SST increases by ~2-8 °C
172 in the North Atlantic between 30°N and 80°N (Fig. 6). The largest increase in ensemble median by 6-8 °C
173 appears in the Labrador Sea on the Cape Farewell (the southernmost point) of Greenland. EC-Earth3-LR
174 simulates the largest increase in the North Atlantic SST above 12°C in the mid-Pliocene experiment (Fig. 4,
175 5).

176 However, the SST increases in the North Atlantic (averaged between 30°N and 80°N) in response to the
177 changes in AMOC maximum and North Atlantic OHT (averaged between 30°N and 80°N) are highly
178 model-dependent (Fig. 5). Of the fifteen PlioMIP2 models, eleven models (CCSM4, CESM1.2, COSMOS,
179 HadCM3, GISS-E2-1-G, IPSLCM5A, IPSLCM5A2, IPSLCM6A-LR, MIROC4m, NorESM1-F, NorESM-L)
180 simulate a mean SST increase between 2 and 4 °C in the North Atlantic. However, the ranges of the changes
181 in AMOC maximum (from 1% to 53%) and mean North Atlantic OHT (from -13% to 43%) are large.
182 Meanwhile, EC-Earth3-LR produces an increase of ~8 °C in mean North Atlantic SST, which is associated
183 with an intensification of 3.2 Sv (19%) in the AMOC maximum and an enhancement of 0.16 PW (41%) in
184 the mean North Atlantic OHT. CCSM4-UoT, CCSM4-Utrecht, CESM2 produce a similar increase of ~5 °C
185 in the mean North Atlantic SST, while the intensification in AMOC maximum shows a large range covering
186 0.9 Sv (4%), 2.1 Sv (11%), and 4.7 Sv (21%), whereas the mean North Atlantic OHT changes by 0.06 PW
187 (9%), 0.04 PW (6%), -0.02 PW (-4%).

188 In PlioMIP2, the surface warming simulated with CCSM4-UoT, CCSM4-Utrecht, CESM2 and
189 EC-Earth3-LR is close to or warmer than the PRISM4 reconstructions (Foley and Dowsett, 2019) in the
190 North Atlantic between 30°N and 80°N, whereas the other models still underestimate the North Atlantic SST
191 (Fig. 6). A previous study (Otto-Bliesner et al., 2017) showed that the closing of the Arctic gateways led to
192 warmer North Atlantic SSTs in the mid-Pliocene experiment, when compared to the pre-industrial. However,
193 in the PlioMIP2 simulations analyzed here the Arctic gateways are closed, while not all models simulate the
194 warm North Atlantic SSTs as reconstructed in the PRISM4 data set (Foley and Dowsett, 2019). Although
195 the Arctic gateways may lead to a better agreement between simulated and reconstructed mid-Pliocene



196 North Atlantic SSTs in some models, the effect is either not present for all of the models or it is not of
197 sufficient amplitude to fully resolve the model-data discord. The PlioMIP2 models show a larger
198 model-spread in the simulated mid-Pliocene SST increases in the high-latitude North Atlantic, as well as the
199 responses in AMOC and North Atlantic OHT, relative to PlioMIP1. This reduced agreement is not surprising
200 as the model spread in global average surface temperatures is likewise more pronounced in PlioMIP2 (1.86–
201 3.60 °C in PlioMIP1 (Haywood et al., 2013) compared to 1.7–5.2 °C in PlioMIP2 (Haywood et al., 2020)).

202

203 **5. Discussion and summary**

204 Compared to the PlioMIP1 ensemble, all PlioMIP2 models forced with the PRISM4 reconstructions
205 that considers closed Arctic gateways simulate an intensification in the mid-Pliocene AMOC. CCSM4,
206 COSMOS, HadCM3, IPSLCM5A, MIROC4m and NorESM-L have all participated in both PlioMIP1 and 2.
207 Simulated with these six models, the increase (compared to the pre-industrial) in the mid-Pliocene AMOC
208 maximum is larger in PlioMIP2 than in PlioMIP1, supporting the suggestion that closed Arctic gateways is a
209 key forcing for the intensified mid-Pliocene AMOC in PlioMIP2. There are several further lines of evidence
210 that support the suggestion. HadGEM3, which carried out the mid-Pliocene experiment forced with the
211 PlioMIP2 boundary conditions, except that the land-sea distribution condition was identical to the
212 pre-industrial, produces a weaker mid-Pliocene AMOC (with a maximum of 14.3 Sv) compared to the
213 pre-industrial (with a maximum of 16.1 Sv). With COSMOS, a sensitivity experiment forced with the
214 modern land-sea distribution (the Arctic gateways opened) also shows a weaker AMOC, when compared to
215 the core mid-Pliocene simulation (Stepanek et al., 2020). As revealed in the early study (Otto-Bliesner et al.,
216 2017), the closed Arctic gateways lead to a stronger AMOC by inhibiting Arctic freshwater export to the
217 North Atlantic. However, the amount in intensification of AMOC due to the closed Arctic gateways seems
218 highly model-dependent, which remains to be shown in more dedicated sensitivity experiments for the
219 PlioMIP2 models.

220 In PlioMIP2, the large-model spread does not support that the intensified mid-Pliocene AMOC is the
221 only forcing responsible for the simulated warm North Atlantic SSTs. Compared to CCSM4, both
222 CCSM4-UoT and CCSM4-Utrecht simulate warmer SSTs in the North Atlantic, indicating that the increased
223 background ocean vertical mixing parameters also contribute to the strong mid-Pliocene North Atlantic
224 warming simulated with these two models. Each model's climate sensitivity also influences the simulated
225 mid-Pliocene warming in PlioMIP2. For example, relative to CCSM4 and CESM1.2, CESM2 has the largest
226 equilibrium climate sensitivity (Feng et al., 2020; Haywood et al., 2020) and simulates the strongest North



227 Atlantic warming in the mid-Pliocene experiment. Moreover, a new lake and soil condition is involved in
228 PlioMIP2 (Haywood et al., 2016). Methods for modifying the soil condition and their impacts on climate in
229 the models are highly model-dependent, due to the large variety of land surface schemes included in the
230 PlioMIP2 models, which could further amplify the diversity of warming signals in high latitude regions.
231 Since not all models carry out the sensitivity experiments designed in PlioMIP2, it remains difficult to
232 distinguish which change in boundary conditions is more dominant for the strong mid-Pliocene North
233 Atlantic surface warming. Earlier energy balance analyses (Hill, 2015; Feng et al., 2017) suggest that the
234 simulated mid-Pliocene North Atlantic warming is dominated by regional radiative feedbacks from changed
235 surface albedo and increased water vapor, instead of the Atlantic OHT, even with an enhanced AMOC by
236 gateway closure.

237 Nevertheless, the PlioMIP2 experiments simulate a sea surface warming that is in better agreement
238 with the PRISM4 reconstructions (Foley and Dowsett, 2019) in the North Atlantic, relative to the PlioMIP1
239 ensemble. As shown in the synthesis paper by Haywood et al. (2020), the multi-model means (with equal
240 weight for each model) agree well with the reconstructions at Sites 609, 1308, and show small differences to
241 the reconstructions at Sites 982, 642. The comparison between the PlioMIP2 simulations and the SST
242 reconstructions in the KM5c interglacial (McClymont et al., 2020) also demonstrates the reduced model-data
243 discord.

244 However, the improved model-data agreement in the North Atlantic is primarily caused by the
245 relatively warm mid-Pliocene simulations run with EC-Earth3-LR and the five models from the
246 CCSM/CESM family (Fig. 6). For the other models, the range of warming at these sites is similar to that of
247 PlioMIP1. This large model-spread suggests that the reconstructed strong mid-Pliocene sea surface warming
248 in the North Atlantic is not necessarily caused by the intensified AMOC and enhanced Atlantic northward
249 OHT as suggested previously (Dowsett, 1992; Raymo et al., 1996). Even given the intensified AMOC in
250 PlioMIP2 due to the closed Arctic gateways, most models underestimate the mid-Pliocene North Atlantic
251 sea surface warming as given by the PRISM4 reconstruction (Foley and Dowsett, 2019).

252 Although the model-data discrepancy is reduced in the North Atlantic partly due to the intensified
253 AMOC, the model-data mismatch remains large in the upwelling regions in PlioMIP2, for example Sites
254 1081, 1082, 1084, 1087 in the Benguela upwelling region (Fig. 6). The PRISM4 (Foley and Dowsett, 2019)
255 and other syntheses of Pliocene SST (Fedorov et al., 2013, McClymont et al., 2020) show that the SSTs are
256 about 6–8 °C warmer than today in the Benguela upwelling region. All PlioMIP2 models underestimate this
257 warming in the PlioMIP2 (Fig. 6). Even EC-Earth3-LR, which produces the warmest mid-Pliocene



258 simulation in the North Atlantic, only simulates 2–4 °C sea surface warming in the Benguela upwelling
259 region.

260 A major feature of the mid-Pliocene seems to be the large increase in SST (about 2–10 °C) in the
261 mid-latitude coastal upwelling regions and the relatively smaller increases in SST (about 2–4 °C) in the mid-
262 to high latitudes (Fedorov et al., 2013) compared to the pre-industrial, though some studies suggest that SST
263 reconstructions in upwelling regions are highly proxy-dependent (e.g., Leduc et al., 2014). For example, in
264 the Benguela upwelling region, the Mg/Ca-based SST is colder than the alkenone-based SST by ~3-10 °C
265 (Leduc et al., 2014). In the California upwelling region, Foley and Dowsett (2019) show that the Pliocene
266 SST is similar to today, whereas Fedorov et al. (2013) show the regional SST is about 2-8 °C warmer than
267 today. Despite the uncertainties in reconstructions, the simulated warming in the mid-latitude upwelling
268 regions in PlioMIP2 can be found in the low end of the proxy-estimated range. Realistic simulations in
269 upwelling regions require good model-abilities in simulating large-scale ocean stratification and sea surface
270 wind stress (Miller and Tziperman, 2017; Li et al., 2019), which are partly model-resolution dependent
271 (Small et al., 2015).

272 Taken together, these model-data discrepancies make it difficult to associate the intensified AMOC and
273 enhanced of Atlantic northward OHT with the reconstructed high mid-Pliocene SSTs. Fedorov et al. (2013)
274 have suggested a possible mechanism for understanding the warm SSTs during the mPWP. Increased mixing
275 in the subtropical ocean and reduced extratropical cloud albedo cause a strong warming in the mid-latitudes,
276 including some upwelling regions. In PlioMIP2, CCSM4-UoT and CCSM4-Utrecht have considered
277 increasing the ocean background mixing parameters, but no model has tested the impact of a reduction of the
278 extratropical cloud albedo in the mid-Pliocene experiments. This mechanism can be further addressed in
279 future to investigate whether it is a suitable candidate for improving the simulation for upwelling regions.

280 Furthermore, it remains problematic to use the intensified AMOC to explain other features of the
281 mid-Pliocene ocean circulation. During the mPWP, the vertical and meridional $\delta^{13}\text{C}$ gradients are reduced in
282 the Atlantic. This can be explained with the increased ventilation in the Southern Ocean and does not
283 necessarily depend on an intensified AMOC (Zhang et al., 2013c). However, simulations of Southern Ocean
284 dynamics are highly model-dependent (Zhang et al., 2013b). In addition to the Southern Ocean, the Pliocene
285 deep ocean circulation in the North Pacific appears different to the present day. In the subarctic North
286 Pacific, high accumulation rates of calcium carbonate and biogenic opal suggest a strong deep convection
287 there, thus the existence of North Pacific deep-water formation and a Pacific meridional overturning
288 circulation (PMOC, Burls et al., 2017). However, with an intensified AMOC, a PMOC remains absent in the



289 PlioMIP2 simulations.

290 In summary, all fifteen coupled models in PlioMIP2 used in this study (CCSM4, CCSM4-UoT,
291 CCSM4-Utrecht, CESM1.2, CESM2, COSMOS, EC-Earth3.3-LR, GISS-E2-1-G, HadCM3, IPSLCM5A2,
292 IPSLCM5A, IPSLCM6A-LR, MIROC4m, NorESM1-F, and NorESM-L) simulate an intensified
293 mid-Pliocene AMOC, relative to the pre-industrial. The simulated AMOC maximum (the maximum of the
294 Atlantic meridional overturning streamfunction) increases by between 1% to 53%. However, these models
295 do not simulate a consistent change in the depth of the Atlantic overturning cell and the Atlantic OHT. The
296 spread in the responses of AMOC and Atlantic OHT in the models becomes larger in PlioMIP2, when
297 compared to PlioMIP1. In the North Atlantic, EC-Earth3-LR and the models from the CCSM/CESM family
298 can simulate an SST increase (~8–12 °C) close to the PRISM4 reconstruction, while other models
299 underestimate the sea surface warming. In PlioMIP2, the model-data discrepancy is reduced in the North
300 Atlantic, but the discrepancy remains large in the upwelling regions. The large model-spread and the
301 remaining model-data discrepancy suggests that an intensified AMOC and an enhanced Atlantic northward
302 OHT, cannot explain the reconstructed warm climate of the mid-Pliocene surface oceans.

303

304

305 **Author contributions**

306 Z.Z. and X.L. analysed the data and wrote the draft of the paper. All authors contributed to discussion of the results and writing of
307 the paper.

308

309 **Competing interests**

310 The authors declare that they have no conflict of interest.

311

312 **Financial support**

313 ZZ, XL were supported by the National Key Research and Development Program of China (Grant No. 2018YFA0605602), the
314 National Natural Science Foundation of China (Grant No. 41888101, 41472160), the Norwegian Research Council
315 (Project No. 221712, 229819, and 262618), the NordForsk-funded project GREENICE (Project No. 61841), as well as
316 computing resources from Notur/Norstore projects NN9133/NS9133, NN9486/NS9486.

317 RF, BLO-B, and ECB acknowledge the CESM project, which is supported primarily by the National Science Foundation (NSF).

318 This material is based upon work supported by the National Center for Atmospheric Research (NCAR), which is a major
319 facility sponsored by the NSF under Cooperative Agreement No. 1852977. This research was additionally sponsored by
320 U.S. National Science Foundation Grants 1903650 and 1814029 to RF and 1418411 to BLO-B. Computing and data
321 storage resources, including the Cheyenne supercomputer (doi:10.5065/D6RX99HX), were provided by the Computational
322 and Information Systems Laboratory (CISL) at NCAR.

323 WRP and DC were supported by Canadian NSERC Discovery Grant A9627 and they wish to acknowledge the support of SciNet
324 HPC Consortium for providing computing facilities. SciNet is funded by the Canada Foundation for Innovation under the
325 auspices of Compute Canada, the Government of Ontario, the Ontario Research Fund – Research Excellence, and the
326 University of Toronto.

327 AvdH and MLJB, acknowledge the program of the Netherlands Earth System Science Centre (NESSC), financially supported



328 by the Ministry of Education, Culture and Science (OCW, grant #. 024.002.001). Simulations with CCSM4-Utr were
329 performed at the SURFsara dutch national computing facilities and were sponsored by NWO-EW (Netherlands
330 Organisation for Scientific Research, Exact Sciences) under the project 17189.
331 GL and CS acknowledge use of computational resources from the Computing and Data Centre of the Alfred-Wegener-Institute –
332 Helmholtz-Centre for Polar and Marine Research towards generation of the COSMOS PlioMIP2 simulation ensemble. GL
333 acknowledges funding via the Alfred Wegener Institute’s research programme PACES2. CS acknowledges funding by the
334 Helmholtz Climate Initiative REKLIM and the Alfred Wegener Institute’s research programme PACES2.
335 QZ acknowledges the financial support by the Swedish Research Council (Vetenskapsrådet, grant no. 2013-06476 and
336 2017-04232). The model simulations with EC-Earth3 and data analysis were performed by resources provided by
337 ECMWF’s computing and archive facilities and the Swedish National Infrastructure for Computing (SNIC) at the National
338 Supercomputer Centre (NSC) partially funded by the Swedish Research Council through grant agreement no. 2016-07213.
339 AMH, SJH and JCT, acknowledge the FP7 Ideas: European Research Council (grant no. PLIO-ESS, 278636), the Past Earth
340 Network (EPSRC grant no. EP/M008.363/1) and the University of Leeds Advanced Research Computing service. JCT
341 was also supported through the Centre for Environmental Modelling And Computation (CEMAC), University of Leeds.
342 WLC and AAO acknowledge funding from JSPS KAKENHI grant 17H06104 and MEXT KAKENHI grant 17H06323, and
343 JAMSTEC for use of the Earth Simulator supercomputer.
344

345 **References**

- 346 Badger, M. P. S., Schmidt, D. N., Mackensen, A. and Pancost, R. D.: High-resolution alkenone palaeobarometry indicates
347 relatively stable pco2 during the pliocene (3.3-2.8 ma), *Philos. Trans. R. Soc. A Math. Phys. Eng. Sci.*, 371(2001),
348 doi:10.1098/rsta.2013.0094, 2013.
- 349 Bragg, F. J., Lunt, D. J., and Haywood, A. M.: Mid-Pliocene climate modelled using the UK Hadley Centre Model: PlioMIP
350 Experiments 1 and 2, *Geosci. Model Dev.*, 5, 1109–1125, <https://doi.org/10.5194/gmd-5-1109-2012>, 2012.
- 351 Burke, K.D., Williams, J.W., Chandler, M.A., Haywood, A.M., Lunt, D.J., and Otto-Bliesner, B.L.: Pliocene and Eocene provide
352 best analogs for near-future climates. *Proc. Natl. Acad. Sci.*, 201809600, 2018.
- 353 Burls, N.J., Fedorov, A.V., Sigman, D.M., Jaccard, S.L., Tiedemann, R., and Haug G.H.: Active Pacific meridional overturning
354 circulation (PMOC) during the warm Pliocene. *Science Advances*, 3(9), e1700156, DOI: 10.1126/sciadv.1700156, 2017.
- 355 Chalk, T.B., De La Vega, E., Foster, G.L., Bysani, R., and Wilson, P.A.: Warming in a warm world: Orbital CO2 forcing variations
356 in the warm Pliocene. Abstract PP21C-1434 presented at the 2018 AGU Fall Meeting, San Francisco, Calif., 11 Dec.2018.
- 357 Chan, W.-L., Abe-Ouchi, A., and Ohgaito, R.: Simulating the mid-Pliocene climate with the MIROC general circulation model:
358 experimental design and initial results, *Geosci. Model Dev.*, 4, 1035–1049, <https://doi.org/10.5194/gmd-4-1035-2011>,
359 2011.
- 360 Chan, W.-L. and Abe-Ouchi, A.: Pliocene Model Intercomparison Project (PlioMIP2) simulations using the Model for
361 Interdisciplinary Research on Climate (MIROC4m), *Clim. Past*, 16, 1523–1545, <https://doi.org/10.5194/cp-16-1523-2020>,
362 2020.
- 363 Chandan, D., and Peltier, W.R.: On the mechanisms of warming the mid-Pliocene and the inference of a hierarchy of climate
364 sensitivities with relevance to the understanding of climate futures. *Clim. Past*, 14, 825-856, 2018.
- 365 Chandan, D., and Peltier, W.R.: Regional and global climate for the mid-Pliocene using the University of Toronto version of
366 CCSM4 and PlioMIP2 boundary conditions. *Clim. Past*, 13, 919–942, 2017.
- 367 Chandler, M. A., Sohl, L. E., Jonas, J. A., Dowsett, H. J., and Kelley, M.: Simulations of the mid-Pliocene Warm Period using two
368 versions of the NASA/GISS ModelE2-R Coupled Model, *Geosci. Model Dev.*, 6, 517–531,
369 <https://doi.org/10.5194/gmd-6-517-2013>, 2013.
- 370 Contoux, C., Ramstein, G., and Jost, A.: Modelling the mid-Pliocene Warm Period climate with the IPSL coupled model and its
371 atmospheric component LMDZ5A, *Geosci. Model Dev.*, 5, 903–917, <https://doi.org/10.5194/gmd-5-903-2012>, 2012.
- 372 Corvec, S., and Fletcher, C.G. Changes to the tropical circulation in the mid-Pliocene and their implications for future climate.



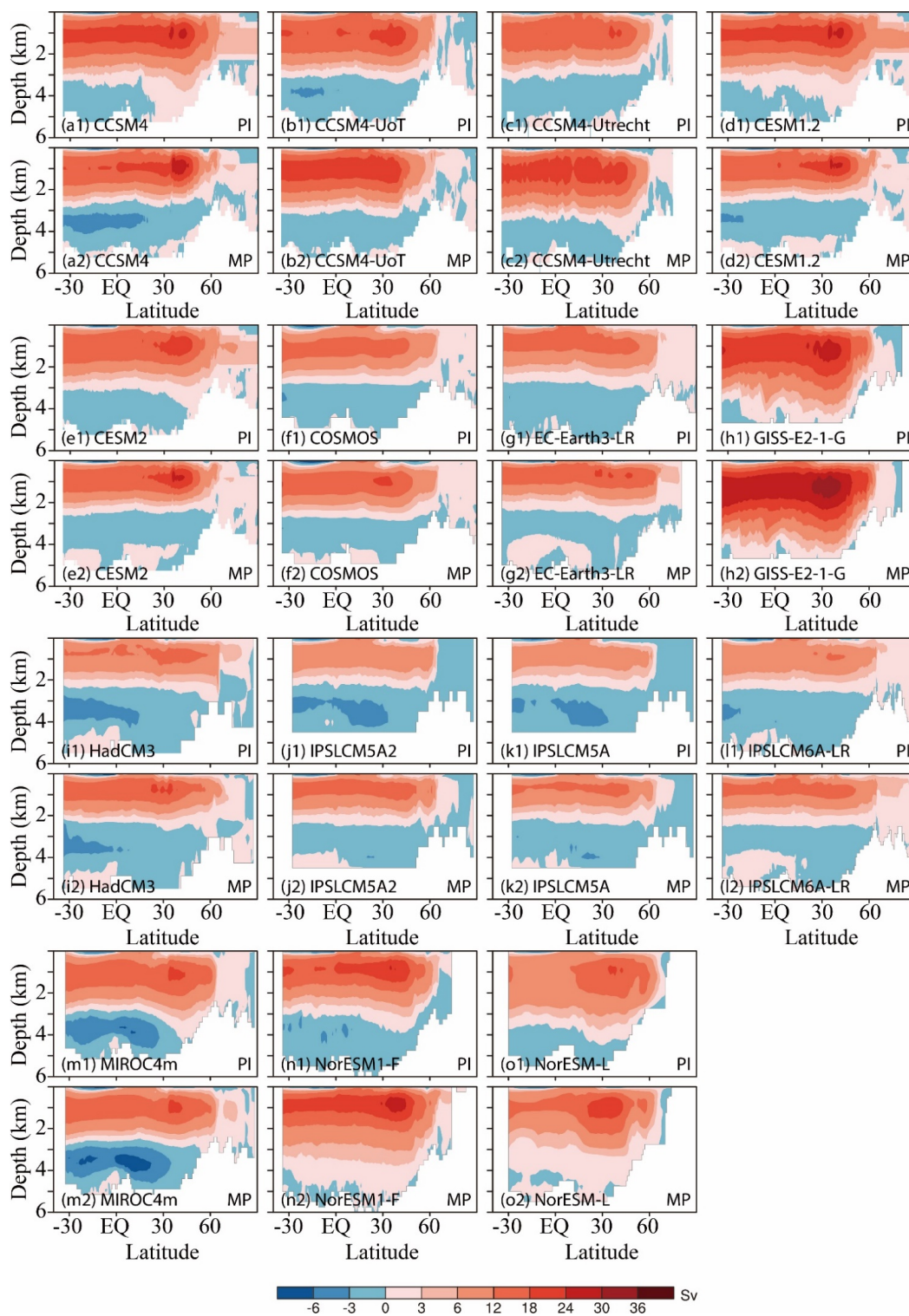
- 373 Clim. Past, 13, 135–147, 2017.
- 374 de Nooijer, W., Zhang, Q., Li, Q., Zhang, Q., Li, X., Zhang, Z., Guo, C., Nisancioglu, K.H., Haywood, A.M., Tindall, J.C., Hunter,
375 S.J., Dowsett, H.J., Stepanek, C., Lohmann, G., Otto-Bliesner, B.L., Feng, R., Sohl, L.E., Tan, N., Contoux, C., Ramstein,
376 G., Baatsen, M.L.J., von der Heydt, A.S., Chandan, D., Peltier, W.R., Abe-Ouchi, A., Chan, W.L., Kamae, Y., and Brierley,
377 C.M.: Evaluation of Arctic warming in mid-Pliocene climate simulations. *Clim. Past Discuss.*, 1–30, 2020.
- 378 Döschner et al., The EC-Earth3 Earth System Model for the Climate Model Intercomparison Project 6. To be submitted to GMD,
379 2020.
- 380 Dowsett, H., Dolan, A., Rowley, D., Moucha, R., Forte, A.M., Mitrovica, J.X., Pound, M., Salzmann, U., Robinson, M., Chandler,
381 M., Foley, K., and Haywood, A.: The PRISM4 (mid-Piacenzian) paleoenvironmental reconstruction. *Clim. Past*, 12, 1519–
382 1538, 2016.
- 383 Dowsett, H., Robinson, M., Haywood, A., Salzmann, U., Hill, D., Sohl, L., Chandler, M., Williams, M., Foley, K., and Stoll, D.:
384 The PRISM3D paleoenvironmental reconstruction. *Stratigraphy*, 7, 123–139, 2010.
- 385 Dowsett, H.J., Cronin, T.M., Poore, R.Z., Thompson, R.S., Whatley, R.C., and Wood, A.M.: Micropaleontological evidence for
386 increased meridional heat transport in the North Atlantic Ocean during the Pliocene. *Science*, 258, 1133–1135, 1992.
- 387 Dowsett, H.J., Foley, K.M., Stoll, D.K., Chandler, M.A., Sohl, L.E., Bentsen, M., Otto-Bliesner, B.L., Bragg, F.J., Chan, W.-L.,
388 Contoux, C., Dolan, A.M., Haywood, A.M., Jonas, J.A., Jost, A., Kamae, Y., Lohmann, G., Lunt, D.J., Nisancioglu, K.H.,
389 Abe-Ouchi, A., Ramstein, G., Riesselman, C.R., Robinson, M.M., Rosenbloom, N.A., Salzmann, U., Stepanek, C., Strother,
390 S.L., Ueda, H., Yan, Q., and Zhang, Z.: Sea Surface Temperature of the mid-Piacenzian Ocean: A Data-Model Comparison.
391 *Sci. Rep.*, 3, 2013.
- 392 Dowsett, H.J., Robinson, M.M., Haywood, A.M., Hill, D.J., Dolan, A.M., Stoll, D.K., Chan, W.-L., Abe-Ouchi, A., Chandler,
393 M.A., Rosenbloom, N.A., Otto-Bliesner, B.L., Bragg, F.J., Lunt, D.J., Foley, K.M., and Riesselman, C.R.: Assessing
394 confidence in Pliocene sea surface temperatures to evaluate predictive models. *Nat. Clim. Change*, 2, 365–371, 2012.
- 395 Fedorov, A.V., Brierley, C.M., Lawrence, K.T., Liu, Z., Dekens, P.S., and Ravelo, A.C. Patterns and mechanisms of early Pliocene
396 warmth. *Nature*, 496, 43–49, 2013..
- 397 Feng, R., Otto-Bliesner, B. L., Fletcher, T. L., Tabor, C. R., Ballantyne, A. P., & Brady, E. C.: Amplified Late Pliocene terrestrial
398 warmth in northern high latitudes from greater radiative forcing and closed Arctic Ocean gateways. *Earth and Planetary
399 Science Letters*, 466, 129–138, 2017.
- 400 Feng, R., Otto-Bliesner, B.L., Brady, E.C. and Rosenbloom, N.: Increased Climate Response and Earth System Sensitivity from
401 CCSM4 to CESM2 in mid-Pliocene simulations. *Journal of Advances in Modeling Earth Systems*, p.e2019MS002033,
402 2020.
- 403 Foley, K.M., and Dowsett, H.J.: Community sourced mid-Piacenzian sea surface temperature (SST) data: US Geological Survey
404 data release, <https://doi.org/10.5066/P9YP3DTV>, 2019.
- 405 Hargreaves, J.C., and Annan, J.D.: Could the Pliocene constrain the equilibrium climate sensitivity? *Clim. Past*, 12, 1591–1599,
406 2016.
- 407 Haywood, A.M., Dowsett, H.J., and Dolan, A.M. Integrating geological archives and climate models for the mid-Pliocene warm
408 period. *Nat. Commun.*, 7, 10646, 2016b.
- 409 Haywood, A.M., Dowsett, H.J., Dolan, A.M., Rowley, D., Abe-Ouchi, A., Otto-Bliesner, B., Chandler, M.A., Hunter, S.J., Lunt,
410 D.J., Pound, M., and Salzmann, U. The Pliocene Model Intercomparison Project (PlioMIP) Phase 2: scientific objectives
411 and experimental design. *Clim. Past*, 12, 663–675, 2016a.
- 412 Haywood, A.M., Dowsett, H.J., Otto-Bliesner, B., Chandler, M.A., Dolan, A.M., Hill, D.J., Lunt, D.J., Robinson, M.M.,
413 Rosenbloom, N., Salzmann, U., and Sohl, L.E. Pliocene Model Intercomparison Project (PlioMIP): experimental design
414 and boundary conditions (Experiment 1). *Geosci. Model Dev.*, 3, 227–242, 2010.
- 415 Haywood, A.M., Hill, D.J., Dolan, A.M., Otto-Bliesner, B.L., Bragg, F., Chan, W.L., Chandler, M.A., Contoux, C., Dowsett, H.J.,
416 Jost, A., Kamae, Y., Lohmann, G., Lunt, D.J., Abe-Ouchi, A., Pickering, S.J., Ramstein, G., Rosenbloom, N.A., Salzmann,
417 U., Sohl, L., Stepanek, C., Ueda, H., Yan, Q., and Zhang, Z. Large-scale features of Pliocene climate: results from the
418 Pliocene Model Intercomparison Project. *Clim. Past*, 9, 191–209, 2013.
- 419 Haywood, A.M., Tindall, J.C., Dowsett, H.J., Dolan, A.M., Foley, K.M., Hunter, S.J., Hill, D.J., Chan, W.L., Abe-Ouchi, A.,



- 420 Stepanek, C., Lohmann, G., Chandan, D., Peltier, W.R., Tan, N., Contoux, C., Ramstein, G., Li, X., Zhang, Z., Guo, C.,
421 Nisancioglu, K.H., Zhang, Q., Li, Q., Kamae, Y., Chandler, M.A., Sohl, L.E., Otto-Bliesner, B.L., Feng, R., Brady, E.C.,
422 von der Heydt, A.S., Baatsen, M.L.J., and Lunt, D.J.: A return to large-scale features of Pliocene climate: the Pliocene
423 Model Intercomparison Project Phase 2. *Clim. Past Discuss.*, 1–40, 2020.
- 424 Hill, D.J., Haywood, A.M., Lunt, D.J., Hunter, S.J., Bragg, F.J., Contoux, C., Stepanek, C., Sohl, L., Rosenbloom, N.A., Chan,
425 W.L., Kamae, Y., Zhang, Z., Abe-Ouchi, A., Chandler, M.A., Jost, A., Lohmann, G., Otto-Bliesner, B.L., Ramstein, G., and
426 Ueda, H.: Evaluating the dominant components of warming in Pliocene climate simulations. *Clim. Past*, 10, 79–90, 2014.
- 427 Hill, D.J.: The non-analogue nature of Pliocene temperature gradients. *Earth Planet. Sci. Lett.*, 425, 232–241, 2015.
- 428 Howell, F.W., Haywood, A.M., Otto-Bliesner, B.L., Bragg, F., Chan, W.L., Chandler, M.A., Contoux, C., Kamae, Y., Abe-Ouchi,
429 A., Rosenbloom, N.A., Stepanek, C., and Zhang, Z.: Arctic sea ice simulation in the PlioMIP ensemble. *Clim. Past*, 12,
430 749–767, 2016.
- 431 Hunter, S.J., Haywood, A.M., Dolan, A.M., and Tindall, J.C.: The HadCM3 contribution to PlioMIP phase 2. *Clim. Past*, 15,
432 1691–1713, 2019.
- 433 Kamae, Y. and Ueda, H.: Mid-Pliocene global climate simulation with MRI-CGCM2.3: set-up and initial results of PlioMIP
434 Experiments 1 and 2, *Geosci. Model Dev.*, 5, 793–808, <https://doi.org/10.5194/gmd-5-793-2012>, 2012.
- 435 Kamae, Y., Yoshida, K., and Ueda, H.: Sensitivity of Pliocene climate simulations in MRI-CGCM2.3 to respective boundary
436 conditions, *Clim. Past*, 12, 1619–1634, <https://doi.org/10.5194/cp-12-1619-2016>, 2016.
- 437 Kanzow, T., Cunningham, S.A., Johns, W.E., Hirschi, J.J.-M., Marotzke, J., Baringer, M.O., Meinen, C.S., Chidichimo, M.P.,
438 Atkinson, C., Beal, L.M., Bryden, H.L., and Collins, J.: Seasonal Variability of the Atlantic Meridional Overturning
439 Circulation at 26.5°N. *J. Climate*, 23 (21): 5678–5698, 2010.
- 440 Leduc, G., D. Garbe-Schönberg, M. Regenberg, C. Contoux, J. Etourneau, and R. Schneider (2014), The late Pliocene Benguela
441 upwelling status revisited by means of multiple temperature proxies, *Geochem. Geophys. Geosyst.*, 15, 475–491, 2014.
- 442 Li, X., Guo, C., Zhang, Z., Otterå, O.H., and Zhang, R. PlioMIP2 simulations with NorESM-L and NorESM1-F. *Clim. Past*, 16,
443 183–197, 2020.
- 444 Li, X., Jiang, D., Tian, Z., and Yang, Y.: Mid-Pliocene global land monsoon from PlioMIP1 simulations. *Palaeogeogr.*,
445 *Palaeoclimatol., Palaeoecol.*, 512, 56–70, 2018.
- 446 Li, X., Jiang, D., Zhang, Z., Zhang, R., Tian, Z., and Yan, Q.: Mid-Pliocene westerlies from PlioMIP simulations. *Adv. Atmos. Sci.*,
447 32, 909–923, 2015.
- 448 Li, Z., Luo, Y., Arnold, N. and Tziperman, E.: Reductions in Strong Upwelling-Favorable Wind Events in the
449 Pliocene. *Paleoceanography and Paleoclimatology*, 34(12), 1931–1944, 2019.
- 450 Lurton, T., Balkanski, Y., Bastrikov, V., Bekki, S., Bopp, L., Braconnot, P., Brockmann, P., Cadule, P., Contoux, C., Cozic, A.,
451 Cugnet, D., Dufresne, J.-L., Ethé, C., Foujols, M.-A., Ghattas, J., Hauglustaine, D., Hu, R.-M., Kageyama, M., Khodri, M.,
452 Lebas, N., Levavasseur, G., Marchand, M., Ottlé, C., Peylin, P., Sima, A. Szopa, S., Thiéblemont, R., Vuichard, N.,
453 Boucher, O.: Implementation of the CMIP6 forcing data in the IPSL-CM6A-LR model. *Journal of Advances in Modeling*
454 *Earth Systems*, 12, e2019MS001940, doi:10.1029/2019MS001940, 2020
- 455 McClymont, E. L., Ford, H. L., Ho, S. L., Tindall, J. C., Haywood, A. M., Alonso-Garcia, M., Bailey, I., Berke, M. A., Littler, K.,
456 Patterson, M., Petrick, B., Peterse, F., Ravelo, A. C., Risebrobakken, B., De Schepper, S., Swann, G. E. A., Thirumalai, K.,
457 Tierney, J. E., van der Weijst, C., and White, S.: Lessons from a high CO₂ world: an ocean view from ~ 3 million years ago,
458 *Clim. Past Discuss.*, <https://doi.org/10.5194/cp-2019-161>, in review, 2020.
- 459 Miller, M.D. and Tziperman, E.: The effect of changes in surface winds and ocean stratification on coastal upwelling and sea
460 surface temperatures in the Pliocene. *Paleoceanography*, 32(4), 371–383, 2017.
- 461 Otto-Bliesner, B.L., Jahn, A., Feng, R., Brady, E.C., Hu, A., and Löffverström, M.: Amplified North Atlantic warming in the late
462 Pliocene by changes in Arctic gateways. *Geophys. Res. Lett.*, 44, 957–964, 2017.
- 463 Pound, M.J., Tindall, J., Pickering, S.J., Haywood, A.M., Dowsett, H.J., and Salzmann, U.: Late Pliocene lakes and soils: a global
464 data set for the analysis of climate feedbacks in a warmer world. *Clim. Past*, 10, 167–180, 2014.
- 465 Raymo, M.E., Grant, B., Horowitz, M., and Rau, G.H.: Mid-Pliocene warmth: stronger greenhouse and stronger conveyor. *Mari.*
466 *Micropaleontol.*, 27, 313–326, 1996.



- 467 Rayner, N.A., Parker, D.E., Horton, E.B., Folland, C.K., Alexander, L.V., Rowell, D.P., Kent, E.C., and Kaplan, A.: Global
468 analyses of sea surface temperature, sea ice, and night marine air temperature since the late nineteenth century. *J. Geophys.*
469 *Res.*, 108(D14), 4407, doi:10.1029/2002JD002670, 2003
- 470 Rosenbloom, N. A., Otto-Bliesner, B. L., Brady, E. C., and Lawrence, P. J.: Simulating the mid-Pliocene Warm Period with the
471 CCSM4 model, *Geosci. Model Dev.*, 6, 549–561, <https://doi.org/10.5194/gmd-6-549-2013>, 2013.
- 472 Salzmann, U., Dolan, A.M., Haywood, A.M., Chan, W.-L., Voss, J., Hill, D.J., Abe-Ouchi, A., Otto-Bliesner, B., Bragg, F.J.,
473 Chandler, M.A., Contoux, C., Dowsett, H.J., Jost, A., Kamae, Y., Lohmann, G., Lunt, D.J., Pickering, S.J., Pound, M.J.,
474 Ramstein, G., Rosenbloom, N.A., Sohl, L., Stepanek, C., Ueda, H., and Zhang, Z.: Challenges in quantifying Pliocene
475 terrestrial warming revealed by data–model discord. *Nat. Clim. Change*, 3, 969–974, 2013.
- 476 Small, R. J., Curchitser, E., Hedstrom, K., Kauffman, B., and Large, W. G.: The Benguela Upwelling System: Quantifying the
477 Sensitivity to Resolution and Coastal Wind Representation in a Global Climate Model, *Journal of Climate*, 28, 9409–9432,
478 [10.1175/jcli-d-15-0192.1](https://doi.org/10.1175/jcli-d-15-0192.1), 2015.
- 479 Stepanek, C. and Lohmann, G.: Modelling mid-Pliocene climate with COSMOS, *Geosci. Model Dev.*, 5, 1221–1243,
480 <https://doi.org/10.5194/gmd-5-1221-2012>, 2012.
- 481 Stepanek, C., Samakinwa, E., Knorr, E., and Lohmann, Gerrit: Contribution of the coupled atmosphere–ocean–sea ice–vegetation
482 model COSMOS to the PlioMIP2, *Clim. Past*, in press, 2020.
- 483 Sun, Y., Ramstein, G., Contoux, C., and Zhou, T. A comparative study of large-scale atmospheric circulation in the context of a
484 future scenario (RCP4.5) and past warmth (mid-Pliocene). *Clim. Past*, 9, 1613–1627, 2013.
- 485 Tan, N., Contoux, C., Ramstein, G., Sun, Y., Dumas, C., Sepulchre, P., and Guo, Z.: Modeling a modern-like pCO₂ warm period
486 (Marine Isotope Stage KM5c) with two versions of an Institut Pierre Simon Laplace atmosphere–ocean coupled general
487 circulation model. *Clim. Past*, 16, 1–16, 2020.
- 488 Yan, Q., Wei, T., Kory, R.L., Kossin, J.P., Zhang, Z., and Wang, H. Enhanced intensity of global tropical cyclones during the
489 mid-Pliocene warm period. *Proc. Natl. Acad. Sci.*, 113, 12963–12967, 2016.
- 490 Zhang, R., Yan, Q., Zhang, Z.S., Jiang, D., Otto-Bliesner, B.L., Haywood, A.M., Hill, D.J., Dolan, A.M., Stepanek, C., Lohmann,
491 G., Contoux, C., Bragg, F., Chan, W.L., Chandler, M.A., Jost, A., Kamae, Y., Abe-Ouchi, A., Ramstein, G., Rosenbloom,
492 N.A., Sohl, L., Ueda, H.: Mid-Pliocene East Asian monsoon climate simulated in the PlioMIP. *Clim. Past* 9, 2085–2099,
493 2013a.
- 494 Zhang, R., Zhang, Z., Jiang, D., Yan, Q., Zhou, X., and Cheng, Z.: Strengthened African summer monsoon in the mid-Piacenzian.
495 *Adv. Atmos. Sci.*, 33, 1061–1070, 2016.
- 496 Zhang, Z. S., Nisancioglu, K., Bentsen, M., Tjiputra, J., Bethke, I., Yan, Q., Risebrobakken, B., Andersson, C., and Jansen, E.:
497 Pre-industrial and mid-Pliocene simulations with NorESM-L, *Geosci. Model Dev.*, 5, 523–533,
498 <https://doi.org/10.5194/gmd-5-523-2012>, 2012.
- 499 Zhang, Z., Nisancioglu, K.H., and Ninnemann, U.S.: Increased ventilation of Antarctic deep water during the warm mid-Pliocene.
500 *Nat. Commun.* 4, 1499, 2013c.
- 501 Zhang, Z.S., Nisancioglu, K.H., Chandler, M.A., Haywood, A.M., Otto-Bliesner, B.L., Ramstein, G., Stepanek, C., Abe-Ouchi, A.,
502 Chan, W.L., Bragg, F.J., Contoux, C., Dolan, A.M., Hill, D.J., Jost, A., Kamae, Y., Lohmann, G., Lunt, D.J., Rosenbloom,
503 N.A., Sohl, L.E., and Ueda, H.: Mid-pliocene Atlantic Meridional Overturning Circulation not unlike modern. *Clim. Past*,
504 9, 14955–11504, , 2013b.
- 505 Zheng, J., Zhang, Q., Li, Q., Zhang, Q., and Cai, M.: Contribution of sea ice albedo and insulation effects to Arctic amplification
506 in the EC-Earth Pliocene simulation. *Clim. Past*, 15, 291–305, 2019.
- 507 Zubakov, V.A., and Borzenkova, I.I.: Pliocene palaeoclimates: Past climates as possible analogues of mid-twenty-first century
508 climate. *Palaeogeogr. Palaeoclimatol. Palaeoecol.*, 65, 35–49, 1988.
- 509
510
511
512

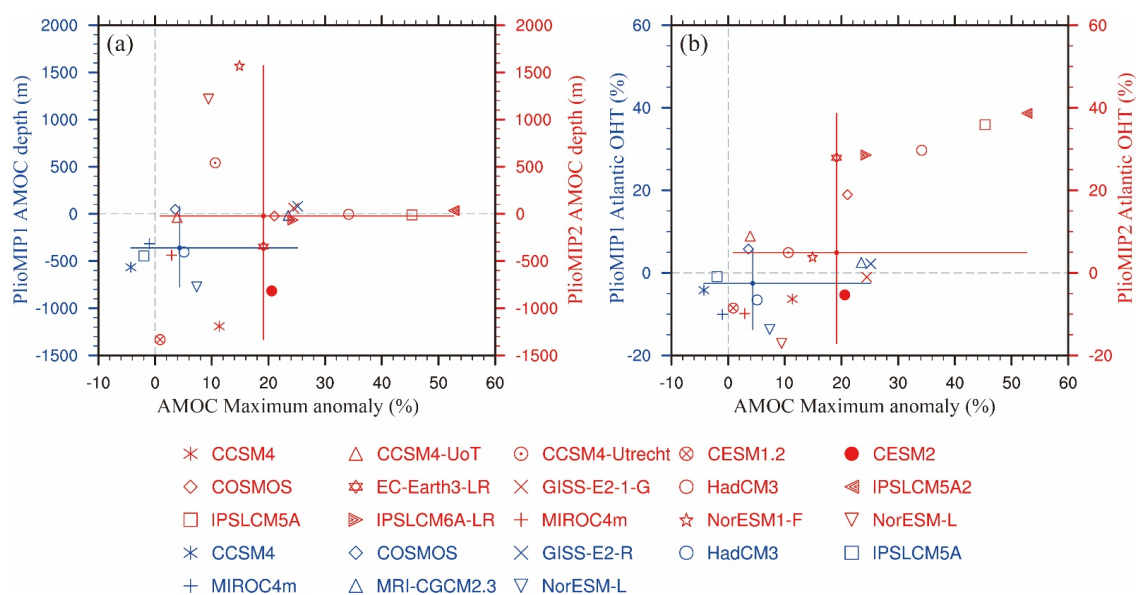


513
 514
 515

Fig. 1. The simulated AMOC (unit: Sv) in PlioMIP2. PI means the pre-industrial. MP means the mid-Pliocene.



516
 517
 518
 519
 520
 521
 522



523
 524
 525
 526
 527
 528
 529
 530
 531
 532
 533
 534
 535
 536
 537

Fig. 2. Simulated changes in AMOC maximum, depth and Atlantic northward OHT. (a) Changes in AMOC maximum (unit: %) vs. responses in the mean depth of AMOC cell (unit: m). (b) Changes in AMOC maximum (unit: %) vs. responses in the mean ocean heat transport in Atlantic between 30 °S and 80 °N (unit: %). The blue markers show the PlioMIP1 simulations. The red markers show the PlioMIP2 simulations. The vertical and horizontal lines show the model range, while the intersection of these lines indicates the median value.



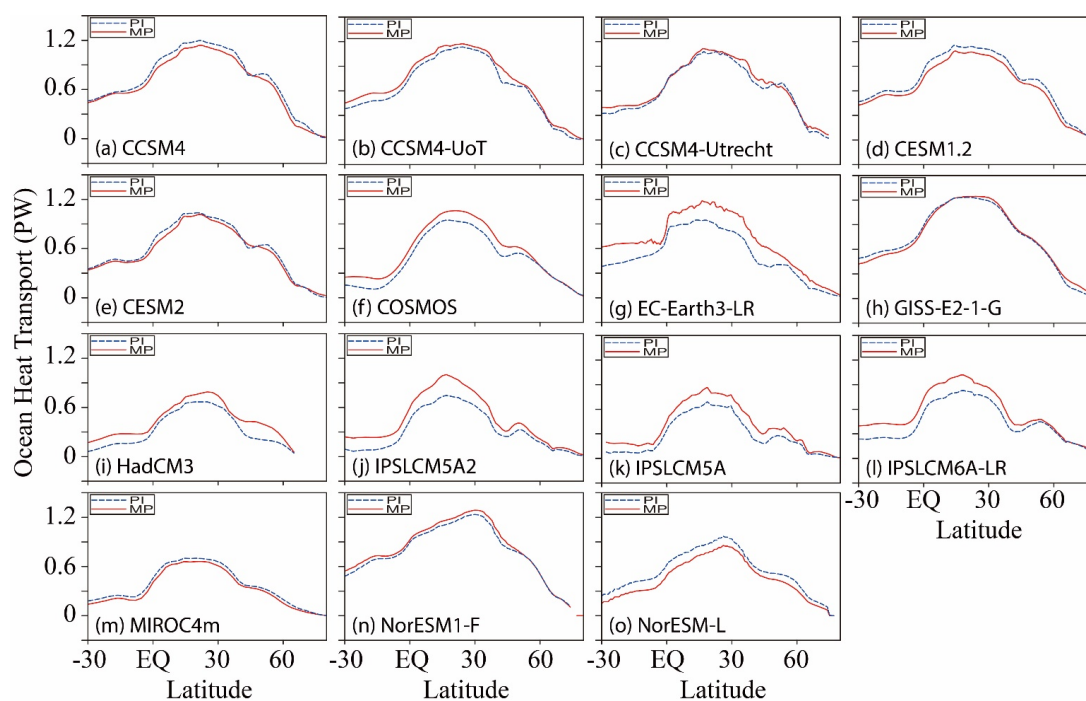
538

539

540

541

542



543

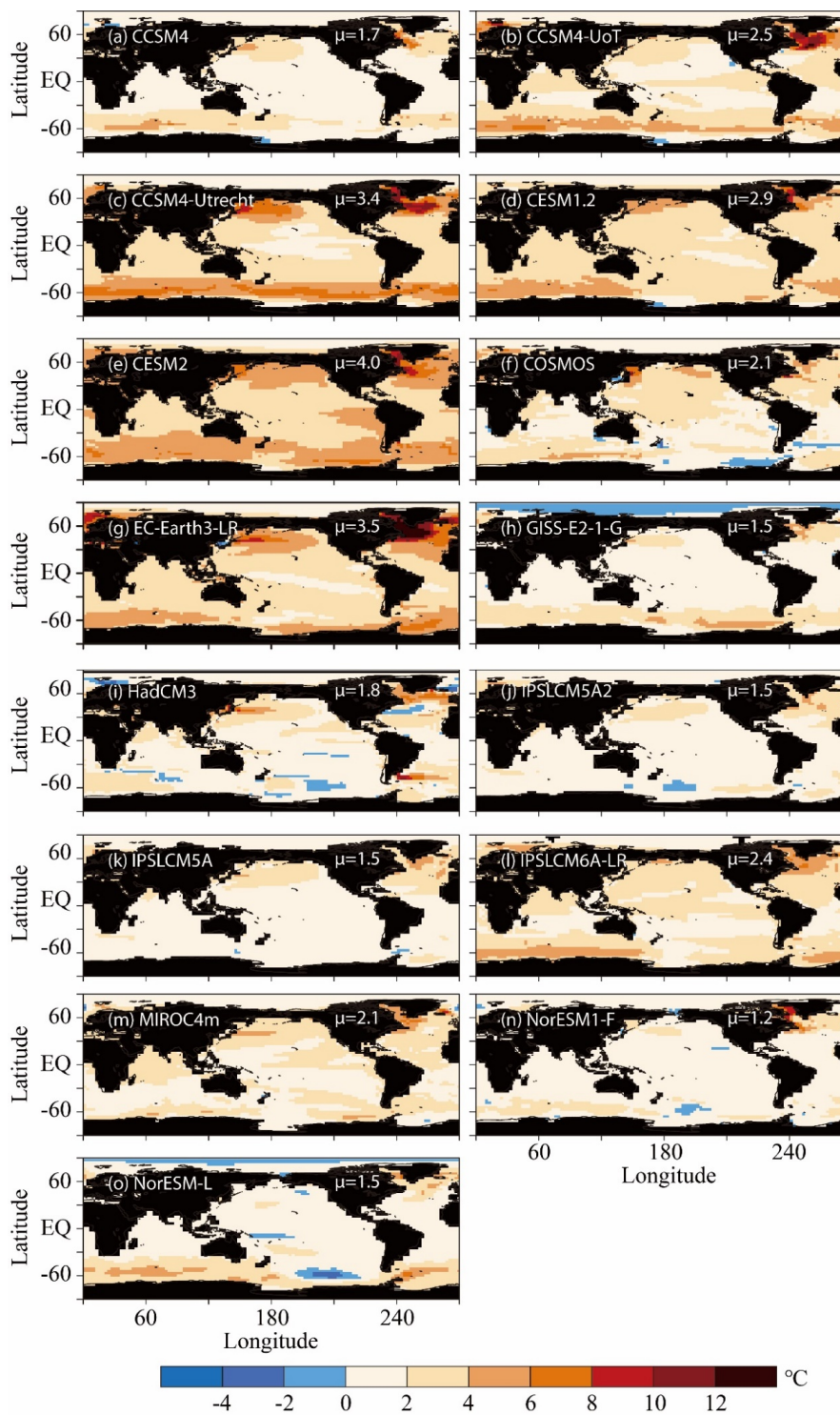
544 **Fig. 3. Simulated Atlantic poleward oceanic heat transport in the PlioMIP2 (unit: PW). Blue dashed**

545 **lines show the pre-industrial, and red solid lines show the mid-Pliocene.**

546

547

548

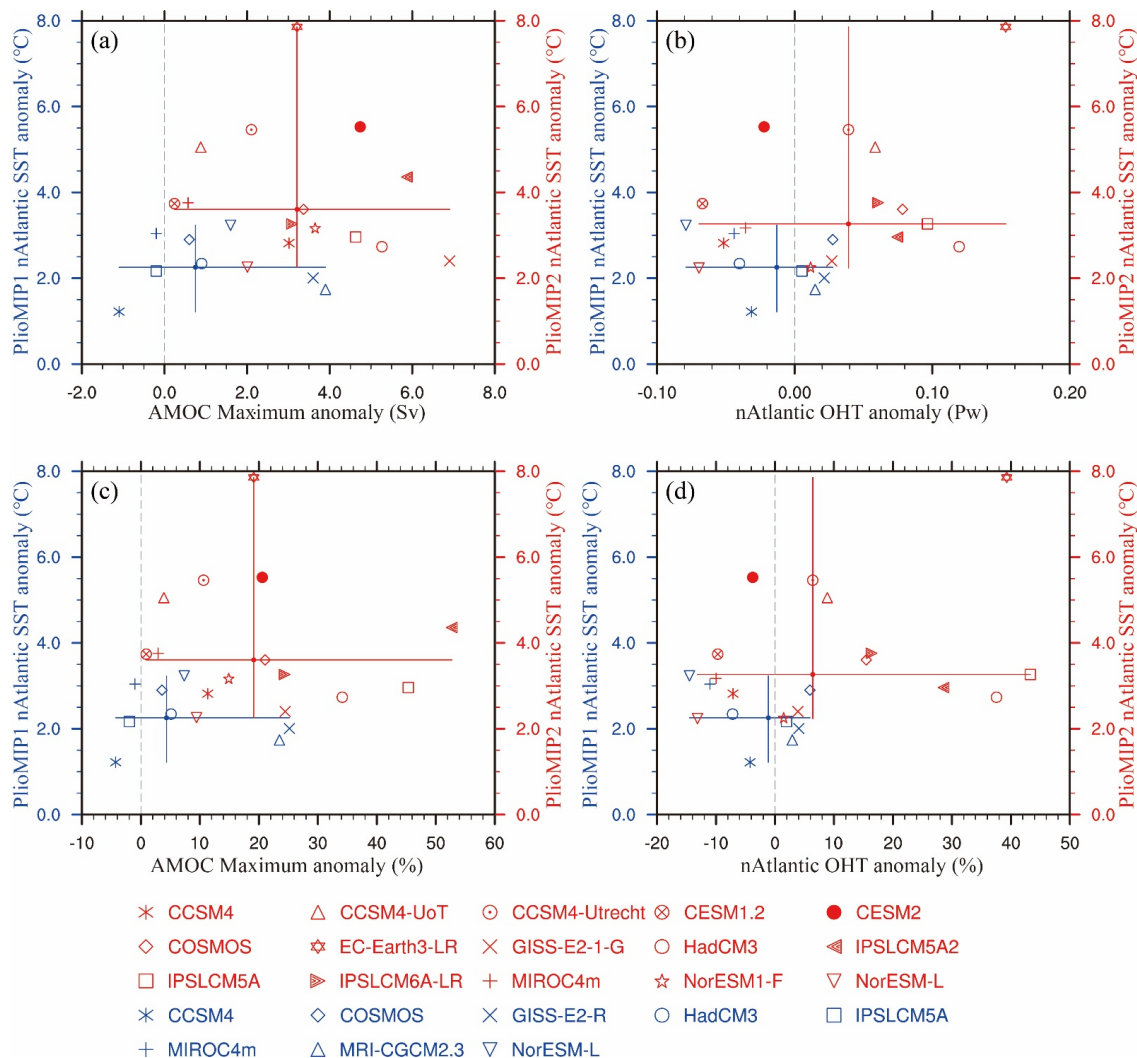


549
 550
 551

Fig. 4. Simulated mid-Pliocene annual SST anomalies in PlioMIP2 (units: °C). μ means the global mean.

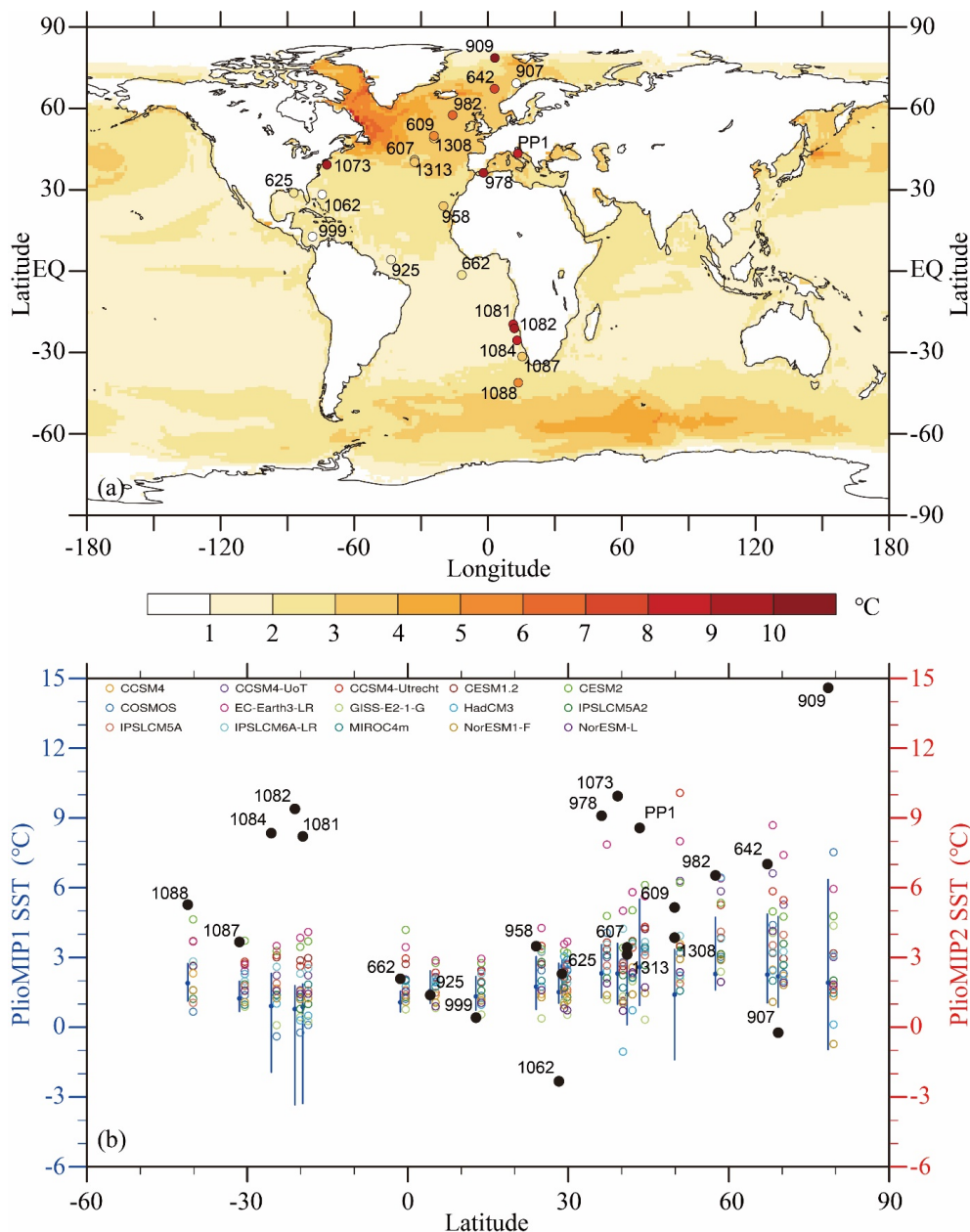


552
 553
 554
 555
 556



557
 558
 559
 560
 561
 562
 563

Fig. 5. Simulated changes in AMOC maximum, North Atlantic OHT, and responses in high-latitude North Atlantic SST. The North Atlantic OHT is the averaged value between 30 °N and 80 °N (unit: Pw). The high-latitude North Atlantic includes the Atlantic and Greenland-Iceland-Norwegian (GIN) seas between 30 °N and 80 °N.



564

565 **Fig. 6. PlioMIP2 and PRISM4 SST comparison in the Atlantic.** (a) PRISM4 SST anomalies and data
 566 sites in the Atlantic and the Mediterranean, against with the multi-model ensemble median of SST anomalies
 567 (the mid-Pliocene vs. the pre-industrial) in PlioMIP2 (unit: °C). (b) Black dots show the PRISM4 SST
 568 anomalies (unit: °C). Vertical blue lines and dots show the PlioMIP1 ranges and median values of changes in
 569 SST for each site. Colored markers show SST changes simulated by each model in the PlioMIP2. The
 570 PRISM4 SST anomalies are calculated based on the PRISM4 mid-Pliocene reconstructions (3.19–3.22 Ma,
 571 Foley and Dowsett, 2019) and the modern observation (1870-1899, Rayner et al., 2003).

572

Table 1. Comparison of PlioMIP2 models.

Model ID	Ocean resolution Lat. × Long.	Background vertical/diapycnal mixing	I. length/mean (years)			Max AMOC			OHT*	OHT**	Reference
			PI	MP	PI	MP	PI	MP	(%)	(%)	
CCSM4	0.27-0.54°×1.1°, L60 depth	default, $k=0.16\times 10^{-4} \text{ m}^2 \text{ s}^{-1}$, latitudinally-varying	>1000/100	1100/100	26.6	29.6	11	-7	-6	Feng et al., 2020	
	0.27-0.54°×1.1°, L60 depth	increased, k from 0.16×10^{-4} to $1\times 10^{-4} \text{ m}^2 \text{ s}^{-1}$, depth dependent	4630/30	1250/30	22.6	23.5	4	9	9	Chandan, et al., 2017, 2018	
CCSM4-Utrecht	0.27-0.54°×1.1°, L60 depth	increased, k from 0.21×10^{-4} to $0.84\times 10^{-4} \text{ m}^2 \text{ s}^{-1}$, depth dependent	3100/100	2048/100	19.8	21.9	11	6	5	Baatsen et al., 2020, in prep.	
	0.27-0.54°×1.1°, L60 depth	default, $k=0.16\times 10^{-4} \text{ m}^2 \text{ s}^{-1}$, latitudinally-varying	>1000/100	1200/100	26.7	27.0	1	-10	-9	Feng et al., 2020	
CESM2	0.27-0.54°×1.1°, L60 depth	default, $k=0.16\times 10^{-4} \text{ m}^2 \text{ s}^{-1}$, latitudinally-varying	1200/100	1500/100	23.0	27.8	21	-4	-5	Feng et al., 2020	
	~3.0°×1.8°, L40 depth	$k=0.105\times 10^{-4} \text{ m}^2 \text{ s}^{-1}$	1950/100	1950/100	16.0	19.4	21	15	19	Stepanek et al., 2020	
EC-Earth3-LR	1.0°×1.0°, L75 depth	$k=0.12\times 10^{-4} \text{ m}^2 \text{ s}^{-1}$	1500/100	1600/100	16.8	20.0	19	39	28	Zhang et al., 2020	
	1°×1.25°, L32 depth	KPP with nonlocal fluxes, $k=0.10\times 10^{-4} \text{ m}^2 \text{ s}^{-1}$	5000/100	3100/100	28.2	35.1	24	4	-1		
HadCM3	1.25°×1.25°, L20 depth	$k=0.10\times 10^{-4} \text{ m}^2 \text{ s}^{-1}$	2999/100	2499/100	15.4	20.7	34	38	30	Hunter et al., 2019	
	0.5-2°×2°, L31 depth	function of turbulent kinetic energy	1500/100	3480/100	11.1	17.0	53	29	39	Tan et al., 2020	
IPSLCM5A	0.5-2°×2°, L31 depth	function of turbulent kinetic energy	650±800/10	3680/100	10.2	14.8	45	43	36	Tan et al., 2020	





IPSLCM6A-LR	1.0° × 1.0°, refined at 1/3° in the tropics, L75 depth	turbulent kinetic energy scheme and an energy-constrained parameterization of mixing due to internal tides	1100/100	1450/100	12.7	15.8	24	16	29	Lurton et al., 2020
MIROC4m	0.56–1.46 × 1.46°, L43 sigma/depth	k from 0.10 × 10 ⁻⁴ to 3 × 10 ⁻⁴ m ² s ⁻¹ , latitudinally varying	2220/100	3000/100	19.6	20.2	3	-10	-10	Chan et al., 2020
NorESM1-F	~1.0° × 1.0°, L53 sigma	k = 0.10 × 10 ⁻⁴ m ² s ⁻¹ , latitudinally varying	2000/100	500/100	24.5	28.1	15	1	4	Li et al., 2020
NorESM-L	~3.0° × 3.0°, L32 sigma	k = 0.10 × 10 ⁻⁴ m ² s ⁻¹ , latitudinally varying	2200/100	1200/100	21.3	23.3	9	-13	-17	Li et al., 2020

574
 575 * North Atlantic ocean heat transport between 30°N and 80°N.

576 ** Atlantic ocean heat transport between 30°S and 80°N.

577 CESM2, EC-Earth3-LR, GISS-E2-1-G and IPSL-CM6A-LR take part in the Coupled Model Intercomparison Project (CMIP) phase 6.

578